Research Article

The Effect of Lunarlike Satellites on the Orbital Infrared Light Curves of Earth-Analog Planets

Nicholas A. Moskovitz,[1] Eric Gaidos,[2] and Darren M. Williams[3]

Abstract

We have investigated the influence of lunarlike satellites on the infrared orbital light curves of Earth-analog extrasolar planets. Such light curves will be obtained by NASA's Terrestrial Planet Finder (TPF) and ESA's Darwin missions as a consequence of repeat observations to confirm the companion status of a putative planet and determine its orbit. We used an energy balance model to calculate disk-averaged infrared (bolometric) fluxes from planet-satellite systems over a full orbital period (one year). The satellites are assumed to lack an atmosphere, have a low thermal inertia like that of the Moon, and span a range of plausible radii. The planets are assumed to have thermal and orbital properties that mimic those of Earth, while their obliquities and orbital longitudes of inferior conjunction remain free parameters. Even if the gross thermal properties of the planet can be independently constrained (*e.g.,* via spectroscopy or visible-wavelength detection of specular glint from a surface ocean), only the largest (∼Mars-sized) lunarlike satellites can be detected by light curve data from a TPF-like instrument (*i.e.,* one that achieves a photometric signal-to-noise ratio of 10 to 20 at infrared wavelengths). Nondetection of a lunarlike satellite can obfuscate the interpretation of a given system's infrared light curve so that it may resemble a single planet with high obliquity, different orbital longitude of vernal equinox relative to inferior conjunction, and in some cases drastically different thermal characteristics. If the thermal properties of the planet are not independently established, then the presence of a lunarlike satellite cannot be inferred from infrared data, which would thus demonstrate that photometric light curves alone can only be used for preliminary study, and the addition of spectroscopic data will be necessary. Key Words: Planetary systems—Planets and satellites: general—Astrobiology—Methods: data analysis. Astrobiology 9, 269–277.

1. Introduction

Planets with a minimum mass of 5–6 Earth masses have recently been detected around low-mass stars (Rivera *et al.,* 2005; Udry *et al.,* 2007), and it seems likely that observatories such as CoRoT or Kepler will detect yet smaller planets (Gillon *et al.,* 2005). Space-based observatories of the future will be capable of directly detecting Earth-sized planets around other stars. Proposed missions include a coronagraph that operates at visible wavelengths (TPF-C) (Traub *et al.,* 2006) and a large-baseline interferometer that operates in the infrared (TPF-I and Darwin) (Fridlund, 2000; Beichman *et al.,* 2006). One goal of such missions is to distinguish between planets that are Earth-like and can support life and those that are decidedly less so (*e.g.,* analogues to Mercury, Venus, or Mars). Several techniques have been proposed to carry out this classification. Spectroscopy can reveal the presence of atmospheric gases, such as H_2O, CH_4, and O_2, which are indicative of temperate conditions or biological activity, or both (Des Marais *et al.,* 2002). Photometry in reflected light can reveal diurnal (rotational) variability associated with ice, oceans, land, and vegetation across the surface of a planet if no clouds are present (Ford *et al.,* 2001). The specular "glint" from oceans might be detected as an increase in the visible flux and polarization of reflected light at large phase angles (Williams and Gaidos, 2008). Selsis (2004) showed that orbital infrared light curves could reveal general thermal properties of terrestrial planets. Gaidos and Williams (2004) showed that diurnally averaged orbital light curves at thermal infrared wavelengths contain information about the thermal properties

[1]Institute for Astronomy and [2]Department of Geology and Geophysics, University of Hawaii at Manoa, Honolulu, Hawaii.
[3]School of Science, Penn State Erie, The Behrend College, Erie, Pennsylvania.

of the planet's emitting layer (surface or clouds) and obliquity. Such light curves would be generated as a by-product of repeated observations to confirm the companion status and orbit of a putative planet and function as a first step toward characterization. One finding of Gaidos and Williams (2004) was that oceans or a thick atmosphere damp seasonal variations in temperature and that low or no variability in a planet's infrared light curve is indicative of the presence of oceans or a thick atmosphere. In conjunction with other characteristics, this is a signature of habitable surface conditions. These authors and the work presented here do not consider the effects of variable cloud cover.

The disk-averaged infrared flux of an orbiting planet can vary, as it presents different phases to a distant observer. This phenomenon has been observed for Jupiter-mass extrasolar planets with semi-major axes much less than 1 AU (Harrington *et al.*, 2006; Cowan *et al.*, 2007; Knutson *et al.*, 2007). The variation in flux from a planet depends on the diurnal pattern of outgoing infrared flux from the emitting surface (either the top of the atmosphere, if any is present, cloud layers, or the surface), which is controlled by the planet's thermal properties and day length. In general, significant day-night temperature differences will occur only if

$$c\omega \lesssim \left(\frac{\partial I}{\partial T}\right)_{\bar{T}} \qquad (1)$$

where c is the heat capacity of the surface/atmosphere, ω is the angular rotation rate, and the right-hand side is the slope of the outgoing bolometric infrared flux at the emitting surface vs. temperature, T, evaluated at the mean surface temperature of the body, $\bar{T}$. For Earth, $c = 8.34 \times 10^7 \, \mathrm{J \, m^{-2} \, K^{-1}}$ and $\partial I/\partial T = 1.58 \, \mathrm{W \, m^{-2} \, K^{-1}}$ for $\bar{T} = 288 \, \mathrm{K}$ (however, the effective emitting temperature of Earth is 255 K). Thus Eq. 1 does not hold for Earth: Earth's day-night temperature variation is small, as it would be for any Earth-like planet with a rotation period much less than a year. This is primarily due to the high heat capacity of the ocean mixed layer, which also moderates surface temperatures over landmasses and controls the outgoing infrared flux budget.

The primordial rotation periods of terrestrial planets are thought to be a stochastic outcome of the final stages of formation by accretion of planetary embryos and will be on the order of hours to days (Lissauer *et al.*, 2000). As a consequence, the disk-averaged infrared flux from an Earth-like planet will only vary significantly along the orbit if the planet has a non-zero obliquity or eccentricity and, hence, seasons. This was explored in Gaidos and Williams (2004).

Earth's moon, lacking an atmosphere or oceans and having a lunar day 29.5 times longer than Earth, experiences a much larger diurnal surface temperature variation. Absence of recent geological activity on the Moon has allowed a regolith of impact ejecta to accumulate. This material is optically dark [the average lunar Bond albedo is 0.07 (Lane and Irvine, 1973) compared to Earth's 0.31] and has a relatively low heat capacity [that of the Moon is $4 \times 10^4 \, \mathrm{J \, m^{-2} \, K^{-1}}$ at 29.5 days or 0.1% of Earth, (Muller and Lagerros, 1998)]. As a result, the inequality of Eq. 1 is satisfied; thus, the Moon makes a significant or even dominant contribution (depending upon viewing geometry) to the variable component of the infrared flux from the Earth-Moon system.

The Moon is thought to have accreted from a circumterrestrial disk of ejecta generated by the impact of a Mars-sized body (Hartmann, 1986). The high ambient temperatures and low gravity in the transient disk explain the Moon's lack of volatiles (Pritchard and Stevenson, 2000). Current scenarios for the final stages of terrestrial planet formation include such giant impacts (Canup and Agnor, 1998), and the results of numerical simulations suggest that they are not rare (Ida *et al.,* 1997). Thus, large satellites that lack atmospheres or oceans may be common around extrasolar rocky planets. Like the Moon, these satellites would have originally formed closer to their parent planets, and their rotations would have quickly synchronized to their orbits (Gladman *et al.*, 1996; Canup and Agnor, 1998). As a result, their diurnal temperature variation could be significant. We note that Moon-sized satellites could retain an atmosphere against gravitational escape over Ga timescales if one was originally present.

Satellites around extrasolar planets will be unresolved by even the most ambitious planet-finding mission; the angular separation of Earth and the Moon at a distance of 10 pc is 0.25 mas. However, a large satellite might reveal itself by a significant variation in the total (bolometric) flux from the system. Such an interpretation would require independent knowledge of the thermal and rotational properties of the parent planet, which can be established via spectroscopy (Des Marais *et al.,* 2002; Selsis, 2004) or optical light curve data (Williams and Gaidos, 2008). If establishment of these gross thermal properties leads to the expectation that infrared flux variation would be small (Eq. 1), then observation of significant variation could be attributed to the presence of a large satellite. In the absence of such auxiliary information, however, the satellite contribution may result in an assignment of erroneous thermal properties to the planet.

We present calculations of infrared light curves of an Earth-like planet with a Moon-like satellite. The terms Earth-like or Earth-analog refer to specific thermal and orbital properties that represent those of Earth (see Section 2). The albedo, heat capacity, and orbital period of the satellite are set to that of the Moon (see above), while its radius is allowed to vary.

In Section 2, we describe the details of the analytical energy balance model (EBM) used in these calculations. We give an illustrative calculation in Section 3. We then determine the minimum radius of a lunarlike satellite that can be detected at infrared wavelengths around an Earth-analog planet (Section 4). In Section 5, we describe the biases in planetary orbital properties that can be introduced by an undetected lunarlike satellite. In Section 6, we describe the effects that low- and high-altitude clouds would have on our calculations, and in Section 7 we discuss the implications of our results.

2. Model

Our calculations are based on the infrared orbital light curve model of Gaidos and Williams (2004). We employed a linearized, analytic EBM to calculate the infrared flux emitted by a planet. This model assumes a single, uniform planetary albedo and parameterizes the thermal inertia and meridional heat transport across a planet's surface. The thermal effect of clouds is accounted for by subtracting a correction term from the outgoing flux (Caldeira and Kasting, 1992). The time-dependent surface temperature distribution is described by a

combination of Legendre polynomials and a Fourier series that are solutions to a diffusion equation with periodic temporal boundary conditions in a spherical coordinate system. The disk-averaged and diurnally averaged infrared flux for a prescribed viewing geometry is calculated along an entire orbit. As long as Eq. 1 is satisfied, diurnally averaging the infrared flux justifies the use of a single, average planetary albedo.

We consider only one set of Earth-like planetary parameters. Although such properties will undoubtedly vary among extrasolar planets, those planets with thermal properties similar to those of Earth will be the most compelling targets of investigation. The thermal inertia of the surface (8.34×10^7 J m^{-2}K^{-1}) and heat diffusion coefficient (0.38 W m^{-2}K^{-1}) were chosen so that, with an albedo ($A = 0.3055$), orbital semi-major axis ($a = 1$ AU), and eccentricity ($e = 0.0167$) of Earth, the model reproduces the meridional surface temperature distribution of Earth as well as the seasonal temperature variation at several latitudes (Gaidos and Williams, 2004).

The orbital properties (a, e, and i) of a real planet can be determined by imaging or astrometry, but the thermal properties of the planet may not be uniquely determined by independent means. We discuss this scenario in Section 7. Under the conditions of known orbital and thermal properties, the light curve is a function of the planet's obliquity (δ_0), the orbital longitude of inferior conjunction relative to the spring equinox (L_0), and the orbital longitude of the apastron (L_{ap}). If the orbit of the planet is nearly circular, then the longitude of apastron L_{ap} (fixed here to 180°) is unimportant.

Ocean and atmospheric circulation and the thickness of an ocean's mixed layer may differ for Earth-like planets with obliquities that are significantly larger than 23.5°. Thus, the actual light curves of such planets would differ from those calculated with Earth-like thermal properties. We examined this effect by comparing general circulation model (GCM) runs for $\delta_0 = 85°$ to our EBM calculations (Fig. 1). The GCM used was the three-dimensional GENESIS 2 model (Williams and Pollard, 2003), and the calculations were performed with $L_0 = 120°$. The amplitude and general shape of the GCM light curves are nearly identical to those of the EBM. However, we find that the phase of the GCM light curves tend to lead those of the EBM by ~35°, with the greatest differences occurring when the geometry of the system is such that the poles of the planet are pointed toward the observer (*e.g.*, high obliquity and high inclination). This is likely due to the inclusion of polar sea ice in the GCM.

The exact origin of the offset in phase is uncertain, but we suspect that it involves effects of seasonal changes in cloud cover, sea ice, or ocean circulation not included in the EBM. In Section 4, we show that artificially adjusting the phase of the EBM light curve (for $i = 60°$) to better match the GCM calculations only slightly increases the probability of satellite detection. In Section 5, we find that this phase lag does not affect the conclusion that an Earth-like planet with a lunarlike satellite produces light curves that resemble those of an isolated planet with high obliquity [*i.e.*, one with large amplitude; see Gaidos and Williams (2004) for a comparison of light curves from Earth-like planets with high and low obliquities]. We are interested only in estimating the detectability of satellites and their gross effect on the interpretation of infrared light curves, rather than on detailed inferences about the climates of planets themselves; thus, we use the
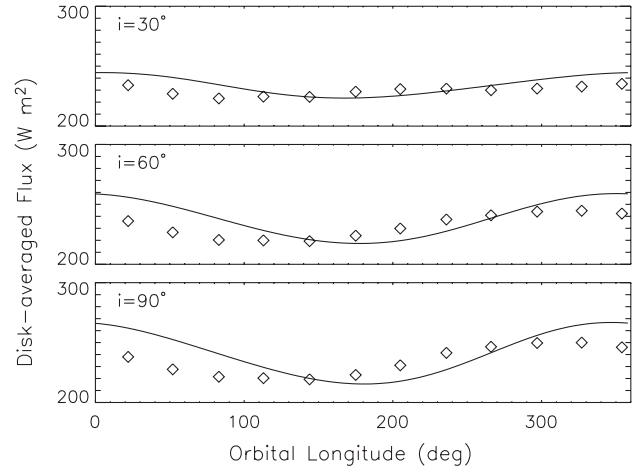
FIG. 1. Calculated EBM (solid) and GCM (diamonds) light curves of a high-obliquity ($\delta_0 = 85°$) planet with Earth-like thermal properties. Light curves are shown for three values of inclination. $L_0 = 120°$ (defined with respect to the vernal equinox) is used for both models. The two models are in close agreement regarding the amplitude of the planetary signal; however, the phase of the EBM calculations tends to lag by ~35°.

EBM to calculate light curves efficiently over a range of obliquity values.

Our formalism for calculating the outgoing infrared flux from a lunarlike satellite is also based upon the analysis in Gaidos and Williams (2004). In the absence of an atmosphere or oceans, the energy-balance equation governing the temperature (T) at a given point on the surface of a satellite with no latitudinal heat transfer is

$$c\frac{\partial T}{\partial t} = S \cdot (1 - A) - I(T), \qquad (2)$$

where time is denoted by t, incident stellar flux by S, albedo by A, and outgoing infrared flux $I(T)$. S and $I(T)$ are calculated as functions of longitude and latitude on the surface of the satellite, taking into account projection effects. To solve this equation analytically, three assumptions are made. First, c is assumed constant in time and across the satellite surface. Second, the temperature dependence of the outgoing infrared flux is approximated as a linearized blackbody:

$$I(T) = I(\bar{T}) \cdot (1 + 4(T - \bar{T})/\bar{T}). \qquad (3)$$

This follows the approach of classical energy balance models (North *et al.*, 1981). Finally, we assume tidally locked, synchronous rotation as is expected for large, collisionally formed satellites (Gladman *et al.*, 1996; Canup and Agnor, 1998). These assumptions allow Fourier series solutions to Eq. 2:

$$T(\theta, \ell) = T_0(\theta) + \sum_{n=1}^{N} [a_n(\theta)\cos(n\ell) + b_n(\theta)\sin(n\ell)], \qquad (4)$$

where T_0 is the mean temperature for a given latitude θ, and ℓ is the longitude on the surface of the satellite. N is set to 10
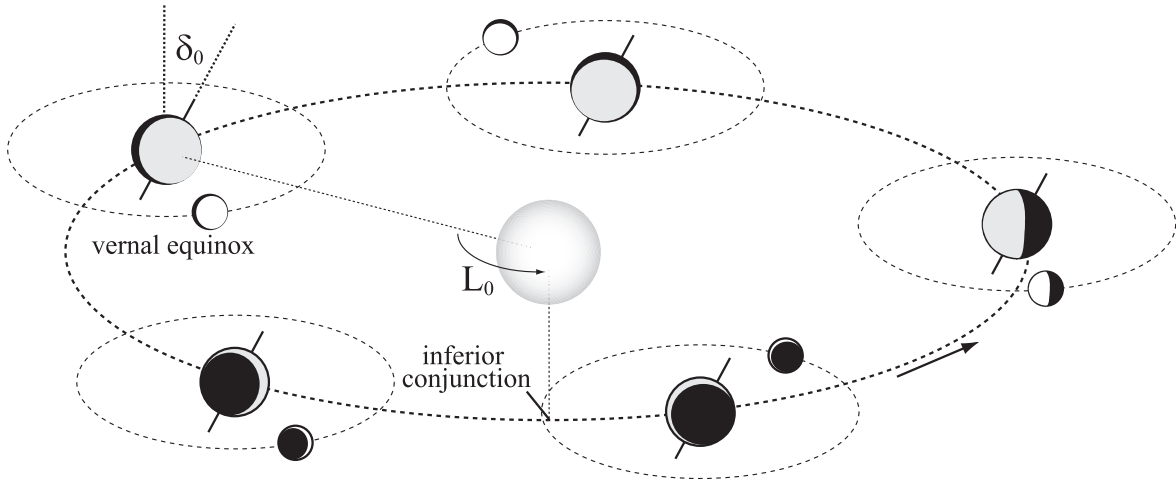
FIG. 2. Planet and satellite at five uniformly spaced orbital longitudes. The vernal equinox corresponds to $L = 0$ and inferior conjunction to $L = L_0$. The disk-averaged flux from the Earth-like planet, which has a high thermal inertia, varies only with seasonal surface temperature differences between the two hemispheres. The disk-averaged flux from the Moon-like satellite, which has a low thermal inertia, depends on its observed phase. The observed phase of the satellite depends only on its orbit around the star, not around the planet.

as numerical tests show that larger values do not significantly change the final light curve. Substitution of Eqs. 3 and 4 into Eq. 2 yields expressions for the Fourier coefficients:

$$a_n(\theta) = \frac{a'_n(B + \alpha) - b'_n \alpha}{\alpha^2 + (B + \alpha)^2} \qquad (5)$$

$$b_n(\theta) = \frac{a'_n \alpha - b'_n(B + \alpha)}{\alpha^2 + (B + \alpha)^2} \qquad (6)$$

where a'_n, b'_n, B and α are

$$a'_n = \int_0^{2\pi} \frac{S(\ell, \theta)}{\pi} \cos(n\ell) d\ell \qquad (7)$$

$$b'_n = \int_0^{2\pi} \frac{S(\ell, \theta)}{\pi} \sin(n\ell) d\ell \qquad (8)$$

$$B = \frac{4I(\bar{T})}{\bar{T}} \qquad (9)$$

$$\alpha = \frac{\omega c}{2} \sqrt{n} \qquad (10)$$

The infrared emission from the surface is calculated with Eq. 3, and the total signal is determined by geometric projection of the hemisphere facing the observer.

For simplicity, we assume that the orbit of the satellite is coplanar with that of the planet's orbit around the star and, because of synchronous rotation, the satellite has zero obliquity. Thus any variation in outgoing flux from the satellite is due to its finite heat capacity. The disk-averaged flux of the satellite is then independent of the location on its orbit around the planet and depends only on the geometric angle described by the star, satellite, and distant observer (Fig. 2).

Variability in the satellite signal is due to its observed phase, which changes with the orbital period of the planet. In Section 4, we consider satellites that differ in size (but not surface properties) from the Moon.

A satellite larger than the Moon will retain heat for a longer time and be more likely to have active volcanism. This could make the satellite darker, as in the case of the lunar mare. However, with an average albedo of 0.07, the Moon is already quite dark. Fresh basalt from active volcanism on the surface of a larger satellite would have little effect on its light curve.

3. Example Light Curves and Observations

Figure 2 illustrates how an Earth-Moon analogue would appear at five evenly spaced points in the system's orbit. In Fig. 3, we have plotted the infrared light curves produced by this system. The bottom panel displays the disk-averaged flux, while the top shows light curves normalized to their respective means. This normalization (which is employed for all subsequent analysis) removes the radius of the planet as a degree of freedom in the model. The calculations were performed assuming an Earth "twin" ($\delta = 23.45°$) with a satellite of radius, orbital period, and albedo equal to that of the Moon [0.273 Earth radii ($R_\oplus$), 29.5 days, and 0.073 respectively]. For these and all simulations, the coplanar orbits of the planet and satellite are inclined by $60°$ with respect to the plane of the sky (the median value of an isotropic distribution). The dotted line in both panels is the contribution from the planet alone. The peak-to-peak amplitude of the satellite's signal (dash-dots in the bottom panel) is $55\,W\,m^{-2}$, whereas the planet's flux alone varies by only $4\,W\,m^{-2}$. Because the thermal inertia of the satellite is low, it displays a larger relative infrared flux variation than that of the planet (Eq. 1). However, because the satellite is smaller, the majority of the average flux originates from the planet.

The assignment of erroneous properties to a planet with an undetected satellite is illustrated in the top panel of Fig. 3, where the dashed line is the best-fit planet-only model to the
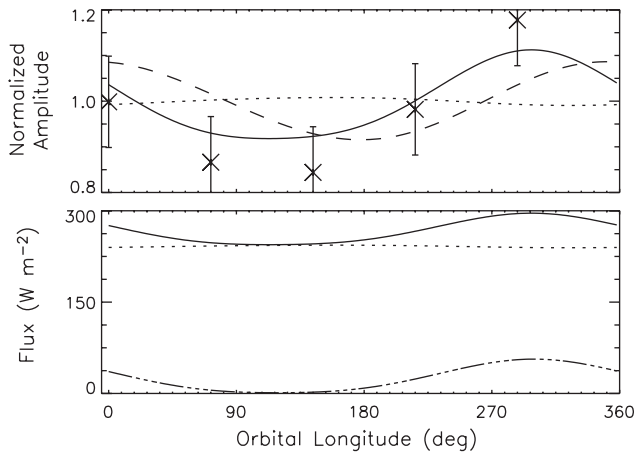
FIG. 3. Simulated light curves and observations of an Earth-Moon "twin." The bottom panel shows disk-averaged flux while the top displays the normalized light curves. In both panels the dotted curve is the planetary seasonal flux and the solid curve is the "true" planet + satellite light curve. The dash-dot curve in the bottom panel is the satellite contribution. In the top panel the sample points are indicated by Xs with one-sigma error bars for a S/N = 10. The best fit, planet-only light curve to the sample points is represented by the dashed line. The top-panel light curves have been normalized by their mean to remove any dependence on the radius of the planet.

planet + satellite observations. This model is of a planet with Earth-like thermal properties and $\delta_0 = 75°$ and $L_0 = 90°$, *i.e.*, quite different than the input values. The phase and amplitude of the light curve produced by these models are not independent, and each depends on the obliquity and orbital longitude of inferior conjunction. Adjusting the orbital longitude of inferior conjunction could produce better agreement with phase but would unacceptably decrease the amplitude of the light-curve. In general, large light curve amplitudes like those produced by Earth-like planets with Moon-like satellites can only be mimicked by single planets with very high obliquities and orbital geometries where the northern or southern hemisphere is pointed toward the observer.

An example of an observation scheme of five evenly spaced measurements is shown in the top panel of Fig. 3. In practice, a minimum of three observations are required to confirm planetary status and reject background sources (Beichman *et al.*, 2006). The TPF mission would conduct a minimum of 3–5 observations on each star during the first two years of a five-year mission. The remaining time would be spent on spectroscopic follow-up of a few dozen planets (Beichman *et al.*, 2006). Spectroscopic observations could, in principle, be split into multiple integrations; however, these would preferentially occur when the planet was near maximum elongation from the star, which would thus maximize the signal-to-noise ratio (S/N). A nulling interferometer (TPF-I, Darwin) or a coronographic imager (TPF-C) will obscure planets along some parts of orbits in the habitable zone (Brown, 2004). We thus consider two observing scenarios, one that consists of five observations at equal longitudinal intervals around the orbit and a second that consists of 14 observation points restricted to half of the orbit farthest from the star. For example, 14×2-day integrations of 36 high-

priority targets might be obtained in three years. Targets in the habitable zone of solar-mass stars [0.9–1.3 AU, Kasting *et al.* (1993)] will have orbital periods of 300–550 days; and, thus, the accessible part of an orbit can be completely observed. For the five-point "confirmation" observation scheme, we assume a S/N ratio of 10 per observation; the median value of the S/N among all 234 stars for which S/N > 5 is achievable for an Earth-sized planet in a 24-hour integration time. For the 14-point "characterization" scheme, we assume a S/N of 20, which will be the case for Earth-sized planets around the nearest 20% of the target stars (Beichman *et al.*, 2006).

4. Satellite Detection Limits

We determine the minimum size of a Moon-like satellite that can be detected around an Earth-like planet whose gross thermal properties are outlined in Section 2. We presume that the inclination of the planet's orbit with respect to the plane of the sky is independently measured by astrometry and use a single value of 60°. For these calculations, the orbital and thermal parameters of the planet and the orbital period, albedo, and thermal inertia of the satellite (assumed to be equal to that of the Moon) are held fixed, while δ_0, L_0, and the satellite radius (R_s) are allowed to vary. With the exception of cases with extremely high planetary obliquity, where most of the planetary signal is at twice the orbital period (Gaidos and Williams, 2004), the signal from the planet and satellite will have the same period. There are then three unknowns (δ_0, L_0, and R_s) but only two measurable quantities: the amplitude and phase of the orbital signal. Thus, it is not possible to disentangle the planetary and satellite signals uniquely. Instead, we define a satellite "detection" as the case where the observations cannot be accounted for by a planet-only model.
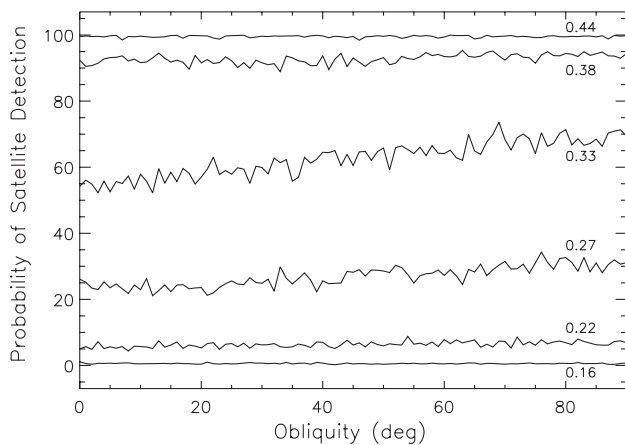
Our detection analysis is as follows: We generate an array of planetary light curves over the full ranges of δ_0 [0–90°] and L_0 [0–360°]. The satellite light curve for a given R_s is calculated and added to each planet light curve in the array. Each total light curve is sampled at N specified points according to either of the observing schemes described in Section 3. Random noise with a given root mean square is added to these measurements. We then perform an exhaustive search of planet-only light curves to find the minimum χ^2 fit to the measurements. The analysis is repeated for different values of R_s. We interpret the confidence level C associated with the value of χ^2 and the number of degrees of freedom as the probability that the deviation from the planet-only model is due to the presence of a satellite. This is because $1 - C$ is the probability that measurements of the light curve of the planet alone would result in a fit with a χ^2 larger than the observed value, *i.e.*, a false positive. We set the effective number of degrees of freedom to the minimum χ^2 value associated with a best fit to N observations of the planet-only light curve. Although this minimum χ^2 value is sensitive to the random noise characteristics of a given sampling, we find that a more robust calculation of the true χ^2 minimum (*i.e.*, averaging over a large number of random noise patterns) produces results that are in close agreement with this single noise characteristic approximation. Our minimum χ^2 approximation produces an increase of nearly an order of magnitude in computational efficiency over the robust method.
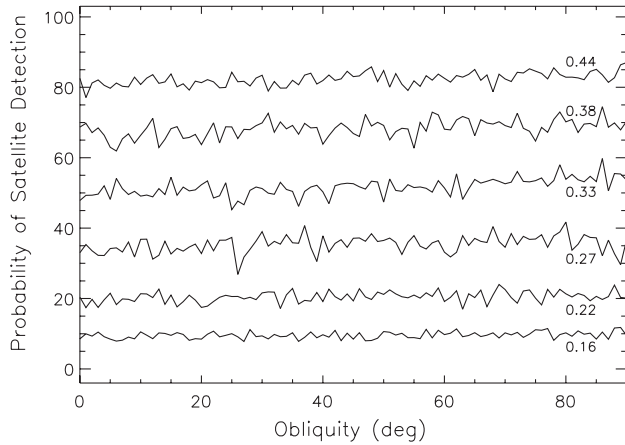
FIG. 4. The L_0 averaged probability of satellite detection as a function of planetary obliquity for a range of satellite radii (0.16, 0.22, 0.27, 0.33, 0.38, and 0.44 planetary radii). The radius of the Moon is 0.27 $R_\oplus$. These simulations were performed with five evenly spaced observations and a S/N of 10. As the radius of the satellite increases, it becomes increasingly difficult to explain the sample measurements with a planet-only light curve; thus the probability of detection increases.
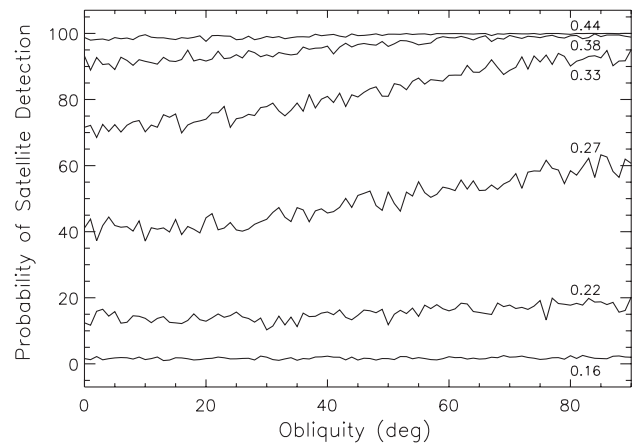
We average C over L_0, which cannot be independently determined for any system but will have a uniform probability distribution. In addition, C is averaged over all possible phases of the measurement scenarios, *i.e.*, the longitudes at which the planet is observed are shifted by 2-degree increments over the orbital phase range $2\pi/N$. This produces an average probability of detection $\langle C \rangle$ for a given R_s and δ_0. The planet's obliquity cannot be independently determined from the light curve of the planet + satellite, nor can it be assumed to have an isotropic distribution (Atobe and Ida, 2007). In Figures 4 and 5, we have plotted $\langle C \rangle$ vs. obliquity for several values of satellite radius (in units of planetary radius). For an Earth-sized planet, this range of radii corre-

sponds to Vesta- to Mars-sized bodies. The two figures correspond to the "confirmation" (5 evenly spaced observations at S/N = 10) and "characterization" (14 observations at S/N = 20 distributed around 50% of the planet's orbit) observation scenarios described in Section 3. As the radius of the satellite increases, the observations become increasingly inconsistent with a planet-only light curve; thus the probability of satellite detection increases. For satellites smaller than 0.33 planetary radii, the probability of detection is lower in the "characterization" observing scheme. This is an effect of the observations being distributed around only 50% of the orbit. The incomplete phase sampling of this scheme does not capture the peak of the satellite flux, which occurs at the longitude of superior conjunction. However, for large satellites ($R_s \geq 0.33$ planetary radii), the amplitude of the net light curve becomes so great that the satellite is detected even without complete phase coverage. The scatter in these probability curves is due to the stochastic noise added to each of the sample measurements. For both observation schemes $\langle C \rangle$ is very weakly dependent on obliquity. These results show that a Moon-like satellite (0.27 $R_\oplus$) would only be detectable with $\sim 30\%$ confidence by either observation scheme. For the "confirmation" and "characterization" observing schemes, a satellite would have to be 0.5 and 0.38 planetary radii, respectively, to be detected with 90% confidence. This corresponds to approximately Mars-sized satellites in orbit around an Earth.

In Fig. 6, we consider how these results would change if a full three-dimensional climate model were used to generate the planetary light curves. As previously stated, our EBM produces light curves that lag by $\sim 35°$ relative to those of the GENESIS 2 GCM for obliquities of 23.5° and 85°. To mimic the results of the GCM, we offset the phase of the EBM light curves by 35° and repeat the analysis of Fig. 5. It would be computationally prohibitive to generate GCM light curves for the full range of obliquities that are included in this analysis; thus, we approximate the GCM by applying this offset. We find that the probability of detection actually increases


FIG. 5. Similar to Fig. 4, except for the "characterization" observing scheme: 14 sample points with a S/N of 20, distributed around 50% of the planet's orbit. Although the S/N is higher than the observations of Fig. 4, the distribution of sample points around only 50% of the orbit makes it difficult to detect satellites of small radii (≤ 0.33 planetary radii).

FIG. 6. Similar to Fig. 5, except that a 35° phase shift has been applied to all EBM planetary light curves so that they agree with the GENESIS 2 GCM. With use of these pseudo-GCM light curves, the detection probability actually increases relative to the EBM case (Fig. 5). This suggests that the EBM places a lower limit on the probability of satellite detection.

slightly with the phase-adjusted pseudo-GCM light curves (Fig. 6). Thus, we conclude that our EBM results are conservative estimates for the probability of satellite detection.

5. Errors Introduced by an Undetected Satellite

As we showed in Fig. 3, the application of planet-only models to a set of observations can result in mischaracterization of the Earth-like planet if a large satellite is present. Even if the gross thermal properties of the planet have been independently established, this will still produce erroneous values of δ_0 and L_0. We describe this effect by recording the "true" (δ_0, L_0) pair for a given planet + satellite light curve and the (δ_0, L_0) pair of the best-fit planet-only light curve as determined by a χ^2 analysis. In some instances, a planet + satellite light curve can be fit with equally low χ^2 by more than one planet-only light curve. For these cases, we choose the (δ_0, L_0) pairs that are closest to the true value. In Fig. 7, we have plotted the direction and proportional magnitude of the error introduced by satellite confusion (the length of the vectors have been reduced for clarity). These simulations were run for an Earth-like planet with a satellite of radius equal to that of the Moon and (for clarity) no intrinsic noise added to the sample points. In nearly all cases, the presence of a lunarlike satellite makes an Earth-analog planet appear to have high (>80°) obliquity. Shifting the planetary light curve phases by 35° to make them resemble the GCM results does not alter the tendency of the best-fit solutions toward high δ_0.

The vectors in Fig. 7 converge toward two values of L_0 (90° and 270°) because the planet-only light curve is in phase with that of the satellite at these L_0. For high-obliquity planets, L_0 values of 90° or 270° translate to a planetary configuration in which the southern or northern hemispheres (respectively) face the observer. At high δ_0, these are the only geometries that produce planet-only light curves with large amplitudes that can reasonably fit a planet + satellite system. Adjusting
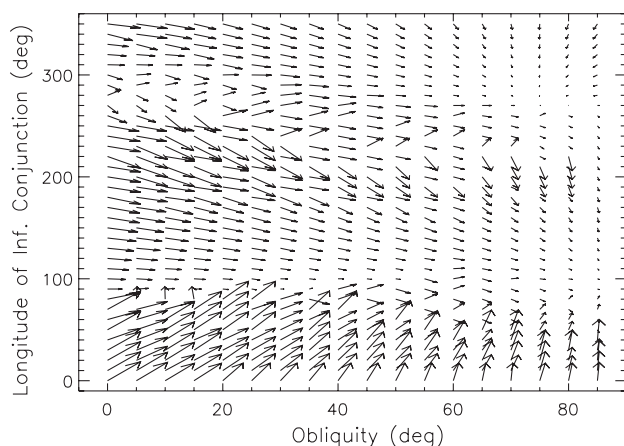
FIG. 7. Error induced in the light curve analysis by an undetected satellite. The vectors point from the true (δ_0, L_0) pair that is used to generate the planet + satellite light curve, toward the best-fit planet-only (δ_0, L_0) pair. For clarity, the length of the vectors has been scaled to the amount of induced error. Their endpoints do not actually fall on the best-fit (δ_0, L_0) values. Nearly all best fit-values cluster at high obliquity and L_0 values of $\sim$90° or $\sim$270°.

for the phase difference between the EBM and the GCM does effect these general trends in L_0. Instead of converging to L_0 values of 90° and 270°, the GCM vector field reaches convergence at L_0 values that are shifted by 35°.

6. The Effect of Clouds

Clouds play an important role in the energy balance and climate of Earth by reflecting sunlight and scattering and trapping long-wavelength radiation; they would presumably do so for Earth-like extrasolar planets as well. Although clouds represent a mean 20 W m^{-2} (8%) gain in radiation for Earth (Hartmann, 1994), we are concerned here only with their seasonal affect on the energy budget and disk-integrated outgoing radiation. These seasonal effects will be most prominent when one hemisphere is presented to the observer. On Earth, low clouds (stratocumulus) produce a decrease in net radiation, while high clouds (cirrus) produce an increase (Hartmann, 1994).

We estimate the thermal effect of seasonal variability in stratocumulus clouds on the light curve of an Earth twin. We assume that these low-altitude clouds radiate at the same temperature as a clear atmosphere and surface, *i.e.*, they produce no additional greenhouse effect. We use a cloud albedo of 0.7 (Hartmann, 1994). Comiso and Stock (2001) estimated variation in cloud cover over the open ocean around Antarctica to vary by only $\pm$1% around a mean of 91%. Seasonal variation of $\pm$10% around a mean of 80% was observed over the North Atlantic (Massons *et al.*, 1998). We adopt a 20% seasonal variation in the mean as a reasonable bracketing value. To produce the global mean Earth albedo of 0.31, a dark ocean ($A = 0.07$) must be covered with 37% clouds. Although the average cloud cover on Earth is $\sim$60%, only half those are low-altitude stratocumulus (Minnis *et al.*, 2002), a value in reasonable agreement with the calculated fraction of 37%. A $\pm$20% fluctuation in the mean coverage produces an albedo variation of 0.047. We assume that the albedo variation is uniformly distributed over each (northern/southern) hemisphere and that it varies sinusoidally in phase with the summer solstice. (This obviously produces a nonphysical discontinuity at the equator, which is unimportant for the purposes of estimating the magnitude of the effect of clouds). We examined the light curves of two cases: one in which an Earth twin is observed at a moderate inclination ($i = 60°$) and the other in which a high-obliquity Earth is observed on an edge-on orbit ($i = 90°$) so that one hemisphere is seen nearly pole-on (results not shown). In both cases, the annual mean of the disk-averaged flux is slightly lower in the presence of low-altitude clouds, but the amplitude and phase of the variation is essentially unchanged. Of course, pathological deviations from terrestrial patterns of cloudiness are possible on planets not quite like Earth, but we have already shown with a GCM model (that includes parameterized cloudiness) that, in at least the high-obliquity regime, our conclusions are not significantly impacted.

For an Earth-like planet, high-altitude clouds will cause a greenhouse effect whose net effect is to offset any decrease in infrared emission caused by their high albedo. Variation in the fraction of high-altitude cloud cover on timescales of less than $\sim$1 day will be averaged over, during typical integrations. We argue that variation in high cloud cover over

longer timescales will be insignificant compared to estimated noise characteristics for a typical observation. High-altitude clouds with a temperature of 210 K would emit ~40% less radiation than the surface. With typical high cloud-cover fractions of ~30% (Minnis *et al.*, 2002) and again assuming ±20% fluctuations in coverage, we calculate that fluctuations in outgoing infrared flux due to high cloud variability will be on the order of a few percent (40% of surface flux ×30% coverage ×20% variability), which would be unresolved by observations with an optimistic S/N of 20. In a more extreme case (*e.g.,* larger variability, greater mean surface coverage, or lower emitting temperatures), the variability in a light curve due to high-altitude clouds will act to further confuse its interpretation.

7. Discussion

The simulations presented here show that time-series infrared photometry by a TPF- or Darwin-like observatory would reveal only the very largest lunarlike satellites (Mars-sized) around Earth-analog planets, and then only if these Earth-like properties, *i.e.,* the presence of oceans or a substantial atmosphere, or both, have been established by independent means, *e.g.,* spectroscopy or optical photometry. This conclusion holds for a wide range of planetary obliquity (Figs. 4, 5, 6), assuming that the approximations of the EBM do not grossly misrepresent the infrared light curve of a high-obliquity Earth-like planet (Fig. 1).

When interpreting infrared light curves, the presence of an undetected lunarlike satellite can suggest erroneous values of planetary obliquity and longitude of inferior conjunction. In the case of a planet with high thermal inertia, inferred values of δ_0 near 90° and L_0 values within 35° of 90° or 270° may indicate the presence of a lunarlike satellite. This result is based on the assumption that the satellite and planetary orbits are coplanar, which may not be the case for high-obliquity planets. Kinoshita (1993) showed that the orbit of a satellite will stay in the equatorial plane of its host planet if the secular rate of change of the planet's obliquity is slower than the precessional speed of the satellite orbital plane. Thus, satellites around planets that experienced rapid changes in obliquity [possibly by collisions as in the case of Uranus (Parisi and Brunini, 1997)] would stay in their coplanar orbits.

If a satellite's orbit is non-coplanar, then its rotation axis will be tilted with respect to the plane of the planet's orbit. This effectively causes a non-zero obliquity for the satellite, which will modify the amplitude of the satellite's light curve but will not change its period. If this non-coplanar orbit precesses, the signal will change over a timescale of many orbital periods.

If the thermal properties of a planet are not independently established via spectroscopy (Des Marais *et al.*, 2002), visible-wavelength detection of glint from an ocean, or significant polarization of visible reflectance (Williams and Gaidos, 2008), then the flux from an unresolved lunarlike satellite can induce serious errors. If the measurements are modeled with the several free parameters (*e.g.,* δ_0, L_0, *A, c* and efficiency of meridional heat transport), then a set of planet + satellite measurements can be satisfactorily fit by a planet-only light curve. For instance, the peak-to-peak light curve amplitude

from a system with a large, unresolved lunarlike satellite around an Earth-analog planet can be fit by a planet with low thermal inertia and drastically different δ_0 and L_0, which implies a planet more akin to Mars than Earth. Such an erroneous inference would impact the determination of the frequency of habitable planets. This reinforces the need for multiple wavelength observations, including spectroscopy and photometry to disambiguate the characterization of extrasolar terrestrial planets (Beichman *et al.*, 2006; Traub *et al.*, 2006).

Where, optimistically, the thermal properties of a planet are known and its satellite is Mars sized, the existence of a satellite may be inferred from infrared data. Such a discovery would provide information about the collisional and kinematic evolution of the parent planet. In addition, a large satellite could be a potential indicator of habitability, as the presence of the Moon is known to stabilize the obliquity and climate of Earth (Laskar *et al.*, 1993).

Acknowledgments

Abbreviations

EBM, energy balance model; GCM, general circulation model; $R_\oplus$, Earth radii, S/N, signal-to-noise ratio; TPF, Terrestrial Planet Finder.

References

Atobe, K. and Ida, S. (2007) Obliquity evolution of extrasolar terrestrial planets. *Icarus* 188:1–17.

Beichman, C., Lawson, P., Lay, O., Ahmed, A., Unwin, S., and Johnston, K. (2006) Status of the Terrestrial Planet Finder interferometer (TPF-I). *Proceedings of SPIE* 6268:62680-S1.

Brown, R.A. (2004) Obscurational completeness. *Astrophys. J.* 607:1003–1013.

Caldeira, K. and Kasting, J.F. (1992) Susceptibility of the early Earth to irreversible glaciation caused by carbon dioxide clouds. *Nature* 359:226–228.

Canup, R.M. and Agnor, C. (1998) Accretion of terrestrial planets and the Earth-Moon system. In *Origin of the Earth and Moon,* edited by K. Righter and R. Canup, Lunar and Planetary Institute, Houston, pp 113–129.

Comiso, J.C. and Stock, L.V. (2001) Studies of Antarctic cloud cover variability from 1981 to 1999. *Proceedings of IGARSS-2004* 4:1782–1785.

Cowan, N.B., Agol, E., and Charbonneau, D. (2007) Hot nights on extrasolar planets: mid-infrared phase variations of hot Jupiters. *Mon. Not. R. Astron. Soc.* 379:641–646.

Des Marais, D.J., Harwit, M.O., Jucks, K.W., Kasting, J.F., Lin, D.N.C., Lunine, J.I., Schneider, J., Seager, S., Traub, W.A., and Woolf, N.J. (2002) Remote sensing of planetary properties and biosignatures on extrasolar terrestrial planets. *Astrobiology* 2:153–181.

Ford, E.B., Seager, S., and Turner, E.L. (2001) Characterization of extrasolar terrestrial planets from diurnal photometric variability. *Nature* 412:885–887.

Fridlund, C.V.M. (2000) Darwin—the infrared space interferometry mission. *ESA Bulletin* 103:20–25.

Gaidos, E. and Williams, D.M. (2004) Seasonality on terrestrial extrasolar planets: inferring obliquity and surface conditions from infrared light curves. *New Astronomy* 10:67–78.

Gillon, M., Courbin, F., Magain, P., and Borguet, B. (2005) On the potential of extrasolar planet transit surveys. *Astron. Astrophys.* 442:731–744.

Gladman, B., Dane Quinn, D., Nicholson, P., and Rand, R. (1996) Synchronous locking of tidally evolving satellites. *Icarus* 122:166–192.

Harrington, J., Hansen, B.M., Luszcz, S.H., Seager, S., Deming, D., Menou, K., Cho, J.Y.-K., and Richardson, L.J. (2006) The phase-dependent infrared brightness of the extrasolar planet ν Andromedae b. *Science* 314:623–626.

Hartmann, D.L. (1994) *Global Physical Climatology*, Academic Press, San Diego.

Hartmann, W.K. (1986) Moon origin—the impact trigger hypothesis. In *Origin of the Moon,* edited by W.K. Hartmann, R.J. Phillips, and G.J. Taylor, Lunar and Planetary Institute, Houston, pp 579–608.

Ida, S., Canup, R.M., and Stewart, G.R. (1997) Lunar accretion from an impact-generated disk. *Nature* 389:353–357.

Kasting, J.F., Whitmire, D.P., and Reynolds, R.T. (1993) Habitable zones around main sequence stars. *Icarus* 101:108–128.

Kinoshita, H. (1993) Motion of the orbital plane of a satellite due to a secular change of the obliquity of its mother planet. *Celestial Mechanics and Dynamical Astronomy* 57:359–368.

Knutson, H.A., Charbonneau, D., Allen, L.E., Fortney, J.J., Agol, E., Cowan, N.B., Showman, A.P., Cooper, C.S., and Megeath, S.T. (2007) A map of the day-night contrast of the extrasolar planet HD 189733b. *Nature* 447:183–186.

Lane, A.P. and Irvine, W.M. (1973) Monchromatic phase curves and albedos for the lunar disk. *Astron. J.* 78:267–277.

Laskar, J., Joutel, F., and Robutel, P. (1993) Stabilization of the Earth's obliquity by the Moon. *Nature* 361:615–617.

Lissauer, J.J., Dones, L., and Ohtsuki, K. (2000) Origin and evolution of terrestrial planet rotation. In *Origin of the Earth and Moon,* edited by K. Righter and R. Canup, Lunar and Planetary Institute, Houston, pp 101–112.

Massons, J., Domingo, D., and Lorente, J. (1998) Seasonal cycle of cloud cover analyzed using Meteosat images. *Annales Geophysicae* 16:331–341.

Minnis, P., Young, D.F., Wielicki, B.A., Sun-Mack, S., Trepte, Q.Z., Chen, Y., Heck, P., and Dong, X. (2002) A global cloud database from VIRS and MODIS from CERES. In *SPIE 3rd International Asia-Pacific Environmental Remote Sensing Symposium, Remote Sensing of the Atmosphere, Ocean, Environment, and Space,* Hangzhou, China. October 23–27, 2002, International Society for Optical Engineering, Bellingham, WA.

Muller, T.G. and Lagerros, J.S.V. (1998) Asteroids as far-infrared photometric standards for ISOPHOT. *Astron. Astrophys.* 338:340–352.

North, G.R., Cahalan, R.F., and Coakley, J.A. (1981) Energy balance climate models. *Rev. Geophys.* 19:91–121.

Parisi, M.G. and Brunini, A. (1997) Constraints to Uranus' Great Collision-II. *Planet. Space Sci.* 45:181–187.

Pritchard, M.E. and Stevenson, D.J. (2000) Thermal aspects of a lunar origin by giant impact. In *Origin of the Earth and Moon,* edited by K. Righter and R. Canup, Lunar and Planetary Institute, Houston, pp 179–196.

Rivera, E.J., Lissauer, J.J., Butler, R.P., Marcy, G.W., Vogt, S.S., Fischer, D.A., Brown, T.M., Laughlin, G., and Henry, G.W. (2005) A ∼7.5 $M_{\oplus}$ planet orbiting the nearby star GJ 876. *Astrophys. J.* 634:625–640.

Selsis, F. (2004) The atmosphere of terrestrial exoplanets: detection and characterization. In *Extrasolar Planets: Today and Tomorrow,* Astronomical Society of the Pacific Conference Series, Vol. 321, edited by J. Beaulieu, A. Lecavelier des Etangs, and C. Terquem, Astronomical Society of the Pacific, San Francisco, CA, pp 170–182.

Traub, W.A., Levine, M., Shaklan, S., Kasting, J., Angel, J.R., Brown, M.E., Brown, R.A., Burrows, C., Clampin, M., Dressler, A., Ferguson, H.C., Hammel, H.B., Heap, S.R., Horner, S.D., Illingworth, G.D., Kasdin, N.J., Kuchner, M.J., Lin, D., Marley, M.S., Meadows, V., Noecker, C., Oppenheimer, B.R., Seager, S., Shao, M., Stapelfeldt, K.R., and Trauger, J.T. (2006) TPF-C: status and recent progress. *Proceedings of SPIE* 6268:62680T.

Udry, S., Bonfils, X., Delfosse, X., Forveille, T., Mayor, M., Perrier, C., Bouchy, F., Lovis, C., Pepe, F., Queloz, D., and Bertaux, J.-L. (2007) The HARPS search for southern extrasolar planets XI. Super Earths (5 & 8 $M_{\oplus}$) in a 3-planet system. *Astron. Astrophys.* 469:L43–L47.

Williams, D.M. and Gaidos, E.J. (2008) Detecting the glint of starlight on the oceans of distant planets. *Icarus* 195:927–937.

Williams, D.M. and Pollard, P. (2003) Extraordinary climates of Earth-like planets: three-dimensional climate simulations at extreme obliquity. *Int. J. Astrobiology* 2:1–19.

Address reprint requests to:
Nicholas A. Moskovitz
Institute for Astronomy
University of Hawaii at Manoa
2680 Woodlawn Drive
Honolulu, HI 96822
USA

E-mail: nmosko@ifa.hawaii.edu